Zdravko Virag[1], Fabijan Lulić[2]

Application of Three Lumped Models of the Arterial Tree to Subjects of Different Age

[1] University of Zagreb, Faculty of Mechanical Engineering and Naval Architecture
[2] University of Zagreb, Pulmonary Disease Clinic

Introduction

The arterial tree is a network of visco-elastic blood vessels, which delivers blood to the whole body. The simplest models of the arterial tree are lumped models, which describe the arterial tree as one or several compliant chambers. The lumped models are attractive for clinicians because they describe the function of the whole arterial tree in terms of simple parameters such as compliance, resistance, and inertance [1]. The main purpose of lumped parameter models is to model the arterial input impedance (the pressure-to-flow ratio in the frequency domain: $Z = p / Q$) as an afterload to the left ventricle. Lumped models are also used to define the total arterial compliance and resistance, which can explain changes in arterial trees due to ageing and diseases.

The goal of this work was to estimate the capability of different lumped models to properly reconstruct arterial tree pressure from the arterial valve flow. We defined three lumped models of the arterial tree: with one, two and three chambers. The models were applied to three typical subjects of different age (adolescent, middle-aged and elderly).

Materials and methods

Fig. 1 shows the measured aortic root pressure and aortic valve flow for the three typical subjects of different age [2].

One-dimensional models of the arterial tree are governed by partial differential equations, which are usually solved numerically. In a numerical procedure the arterial tree is divided into a number of short elements of different diameter and wall properties. In the case of the Voigt model for the arterial wall, each element can be considered as a chamber defined by the compliance and wall resistance (viscosity), while inertance and resistance characterize the flow along the chambers. By reducing the number of elements in a one-dimensional model to one or a few, a lumped model is obtained. Such reduction from one-dimensional to the lumped model is appropriate when the wave speed tends to infinity [3] (in real problems when the product of wave speed and heart period is much greater than the length of the aorta).

Here we used three lumped parameter (or Windkessel) models consisting of one, two and three chambers, which are defined by three (WK3), six (WK6) and nine (WK9) parameters, respectively. Fig. 2 shows the electrical analogue schemes of the selected Winkessel models. In the WK3 model (also called viscous Windkessel [4]) C_0 and η_0 define the visco-elastic chamber and R represents the peripheral resistance. It is clear that the one-chamber Windkessel model cannot describe any travel or reflection of pressure wave. That is why we chose WK6 and WK9 models, which consist of two and three chambers, respectively. The WK6 model is an extended five element model [5] (extension is resistance r_1), while the WK9 model can be considered as a step toward the one-dimensional model, and it is not used in literature, probably because it contains too many parameters for a lumped model. In a Windkessel model with at least two chambers there is a mass redistribution between chambers and such a model can mimic elementary pressure wave reflection. For example, in the WK6 model a visco-elastic chamber (defined by C_0 and η_0

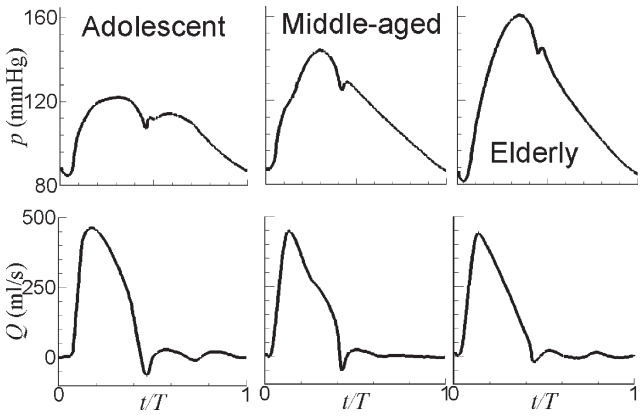

Fig. 1. Recorded aortic root pressure (top) and aortic valve flow (bottom down) for three subjects of different age (T is heart period)

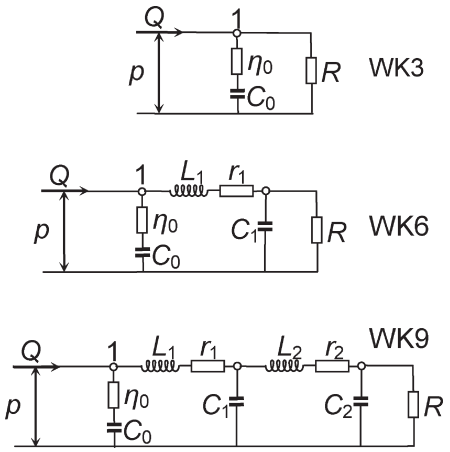

Fig. 2. Electrical analogue schemes of the selected lumped models of the arterial tree

as in the WK3 model) is connected by inertance L_1 and resistance r_1 with the other, purely elastic chamber (defined by C_1). Peripheral resistance R has a similar meaning as in the case of the WK3 model. Unfortunately, there is no unambiguous explanation what these two chambers in the WK6 model represent. They can be two parts of large arteries or the first chamber can represent large arteries, while the second one represents small arteries. The same applies to the WK9 model.

The measured aortic valve flow is applied at the inlet (at point 1 in Fig. 2). The input pressure is calculated by using the model. The model parameters are obtained by minimizing the pressure root mean squared error (RMSE) defined as

$$\mathrm{RMSE} = \sqrt{\sum_1^n \left(p - p^{\mathrm{calc}}\right)^2 / n}\,, \qquad (1)$$

where p^{calc} and p are the calculated and the measured aortic root pressure, respectively, and n is the number of time instants during the heart period at which the pressure is measured.

In the cases of the WK6 and the WK9 models, there are several local minima, and the solution depends on the starting point. To increase a chance to find the point with the absolute RMSE minimum we calculated the RMSE at a number of randomly selected points within the parameter domain, and for the starting point, we chose the one with the minimal RMSE.

Results and Discussion

The model parameters are identified from the measured data for three subjects (Fig. 1). Table 1 shows the values of the obtained parameters for all models and the achieved RMSE values. Fig. 3 illustrates the ability of the models to reconstruct the measured pressure from the measured flow, as well as the comparison between the measured and calculated input impedance.

Table 1 shows that the arterial compliance C_0 decreases with ageing (according to all models) and peripheral resistance increases. Because of reduced compliance the wave speed increases, and a Windkessel model becomes more appropriate [6]. This is an explanation why the WK3 model reconstructs the measured pressure better (with lower RMSE) in the case of the elderly subject than in the case of the middle-aged or the adolescent one. In the case of the adolescent subject, the wave speed is low and the pressure wave reflection at the aortic root occurs during diastole (see the secondary pressure rise in Fig. 1), when the aortic valve flow is equal to zero. The WK3 model cannot describe such phenomena and a Windkessel model with more chambers (or even better a one-dimensional model) is required. Table

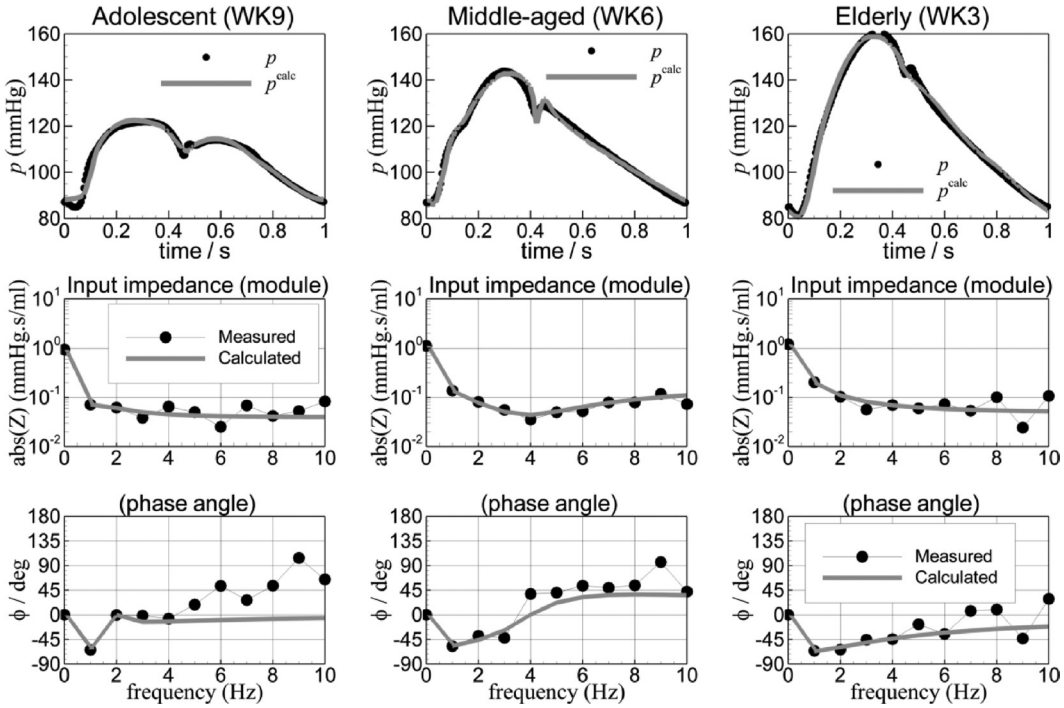

Fig. 3. Measured and calculated pressure for the three subjects and the measured and the calculated input impedance (modulus and phase angle)

Table 1. The obtained values of the model parameters for three subjects (C_0, C_1 and C_2 are expressed in ml/mmHg; η_0, r_1, r_2 and R in mmHg·s/ml; L_1 and L_2 are in mmHg·s²/ml; RMSE is in mmHg)

Subject:	Adolescent			Middle-aged			Elderly		
Model:	WK3	WK6	WK9	WK3	WK6	WK9	WK3	WK6	WK9
C0	2.538	1.708	2.213	1.239	0.738	0.624	0.769	0.412	0.202
10η0	0.401	0.423	0.393	0.617	1.853	2.075	0.504	1.199	0.702
1000L1		19.49	8.638		2.848	3.070		2.360	1.512
10r1		0.000	0.146		0.516	0.375		0.630	0.637
C1		0.436	2.965		0.593	0.579		0.383	0.661
1000L2			13.85			43.86			113.6
10r2			0.000			0.000			0.992
C2			5.584			0.107			0.096
R	0.908	0.908	0.893	1.116	1.064	1.078	1.202	1.139	1.039
RMSE	4.00	1.89	1.52	2.73	1.52	1.21	1.57	1.22	0.84

1 shows that the level of RMSE of less than 1.6 mmHg is obtained for the adolescent subject by the WK9 model, for the middle-aged subject by the WK6 model and for the elderly subject by the WK3 model. The one chamber model is appropriate for the arterial tree of older subjects (with stiffer aorta), and in the case of younger subjects, a lumped model with two or three chambers is a better choice.

References

[1] Westerhof N., Lankhaar JW., Westerhof B.E.: The arterial Windkessel. Med. Biol. Eng. Comput. (2009) 47:131–141.

[2] Nichols W.W., O'Rourke M.F.: McDonald's Blood flow in Arteries. Theoretical, experimental and clinical principles, (2005) 5th ed., Arnold, London.

[3] Christopher C. M., Berger D. S., Noordergraaf A.: Apparent arterial compliance, Am. J. Physiol. 274 (Heart Circ. Physiol. 43): H1393–H1403, 1998.

[4] Burattini R., Natalucci S.: Complex and frequency-dependent compliance of viscoelastic windkessel resolves contradictions in elastic windkessels, Medical Engineering & Physics 20, 502–514, 1998.

[5] Toy S. M., Melbin. J., Noordergraaf A.: Reduced Models of Arterial Systems, IEEE Transactions on Biomedical Engineering, Vol. BME-32, No. 2, 174-176, and 1985.

[6] Mohiuddin M. W., Laine G. A., Quick C. M.: Increase in pulse wavelength causes the systemic arterial tree to degenerate into a classical windkessel, Am J Physiol Heart Circ Physiol 293: H1164–H1171, 2007.

Ivan Korade, Zdravko Virag and Mario Šavar

Numerical Simulation of One-dimensional Blood Flow in Elastic and Viscoelastic Arterial Network

University of Zagreb, Faculty of Mechanical Engineering and Naval Architecture

Introduction

Numerical simulation of blood flow in the arterial tree is challenging due to difficulties in describing the gemetry, nonlinear wall viscoelasticity, and non-Newtonian rheological properties of blood. One-dimensional models present a good compromise between Windkessel and three-dimensional models [1, 2]. Numerical simulation of arterial flow is very useful for the thorough understanding of pressure and flow waves propagation phenomena.

The goal of this paper is to present a method of characteristics (MOC) [3, 4] for solving a nonlinear one-dimensional model in an arterial tree with elastic and viscoelastic wall. The developed method was applied to the 37-element silicone model of arterial tree with available experimental data [5]. The test was used in [6] to check the ability of the mathematical model and the numerical scheme of correctly describing the multiple reflections from multiple outflow and junction conditions. Here we used this benchmark to verify the in-house developed code by comparing the obtained results with the experimental data and with the results of other methods.

Mathematical model

A one-dimensional model of blood flow in a pipe with viscoelastic wall reads [6]:

$$\frac{\partial A}{\partial t}+\frac{\partial Q}{\partial x}=0\,, \tag{1}$$

$$\frac{\partial Q}{\partial t}+\frac{A}{\rho}\frac{\partial p}{\partial x}+\frac{\partial (Qv)}{\partial x}=-fQ\,, \tag{2}$$

$$p - p_0 = \frac{1}{C_D}(\sqrt{A} - \sqrt{A_0}) + \eta \frac{\partial A}{\partial t}, \qquad (3)$$

where x, t are the space and the time coordinate, respectively, A is cross-sectional area ($A = D^2\pi/4$), Q is volume flow rate, and $v = Q/A$, p is transmural pressure, ρ is fluid density, A_0 is constant cross-sectional area at a constant pressure of p_0. Coefficients f, C_D and η are defined by:

$$f = \frac{2(\zeta+2)\pi\mu}{\rho A}, \quad C_D = \frac{3A_0}{4\sqrt{\pi}E\delta} \text{ and } \eta = \frac{\tau}{2C_D\sqrt{A}}, \qquad (4)$$

where μ is fluid viscosity, ζ is constant for particular velocity profile, E is elastic modulus and τ is retardation time constant in the Voigt model.

Numerical method

The artery is discretized into a number of elements of length Δx. Fig. 1 shows two typical elements (denoted by j and k) bounded by nodes (I, J, and K). The pressure is defined at the nodes, A is defined in the middle of each element (and it is considered to be constant along the element) and Q is defined at each end of each element. Thus, four unknowns are stored for each element. For example, the unknowns related to the element j are p_J, Q_{jL}, Q_{jD} and A_j, as shown in Fig. 1.

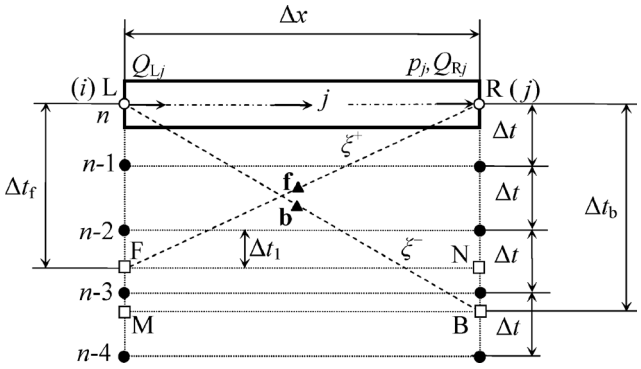

Fig. 1. An element of a discretized arterial tree with the arrangement of variables. For each element, three variables are stored: pressure p_j, flow rate Q_{Rj} at the element outlet, and Q_{Lj} at the element inlet. The time instances are denoted by n, n-1, n-2, n-3, and n-4. Dashed lines denote the characteristics defined by $\xi^+ = v + c$ and $\xi^- = v - c$; empty circles denote the nodes at the new instance at which unknowns should be calculated; filled circles denote nodes at older time instances at which the values of all variables are known from the previous integration steps; squares denote the interpolation points F and B on the forward and backward characteristic lines, and the auxiliary interpolation points N and M are at the same time instances as the points F and B, respectively; triangles denote midpoints f and b of the forward and backward characteristics, respectively

By using Eq. (3), Eqs. (1) and (2) can be transformed into a set of compatibility equations, which are valid along two characteristic lines defined by $\xi^{\pm} = v \pm c$ in the form:

$$\frac{1}{C}\mathrm{d}Q^{\pm} - (v \mp c)\,\mathrm{d}p^{\pm} = -\frac{1}{C} f Q \mathrm{d}t - v^2 \eta \frac{\partial^2 A}{\partial x \partial t}\mathrm{d}t + (v \mp c)\eta \frac{\partial^2 Q}{\partial x \partial t}\mathrm{d}t, \qquad (5)$$

where $C = 2C_D\sqrt{A}$, and $c = \sqrt{A/(\rho C)}$ is wave speed. We establish relationship between pressure and area from the discretized form of Eq. (3), which serves to exclude A from the set of unknowns. The third equation related to each node is the continuity equation. For example, at node R in Fig. 2, this equation reads:

$$Q_{Rj} = Q_{Wj} + \sum_{k=1}^{N_{out}} Q_{Lk}, \qquad (6)$$

where Q_{TJ} is the branching flow from the large artery into a small one, which is modeled by the inertial four element Windkessel as depicted in Fig. 2. In this model, L_J is inertance, r_J is resistance, C_{TJ} is the capacity of branching arteries and R_J is the peripheral resistance at node J.

We discretized Eq. (5) and all other auxiliary equations by using second order accuracy, and the resulting system of algebraic equation is solved by a direct method. The

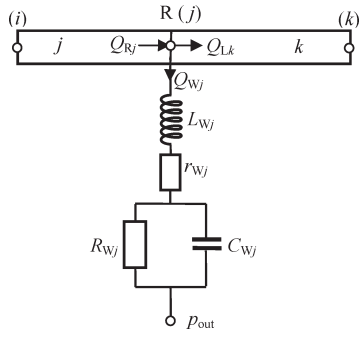

Fig. 2. Electrical analogue scheme of the Windkessel model defining the node outlet boundary condition

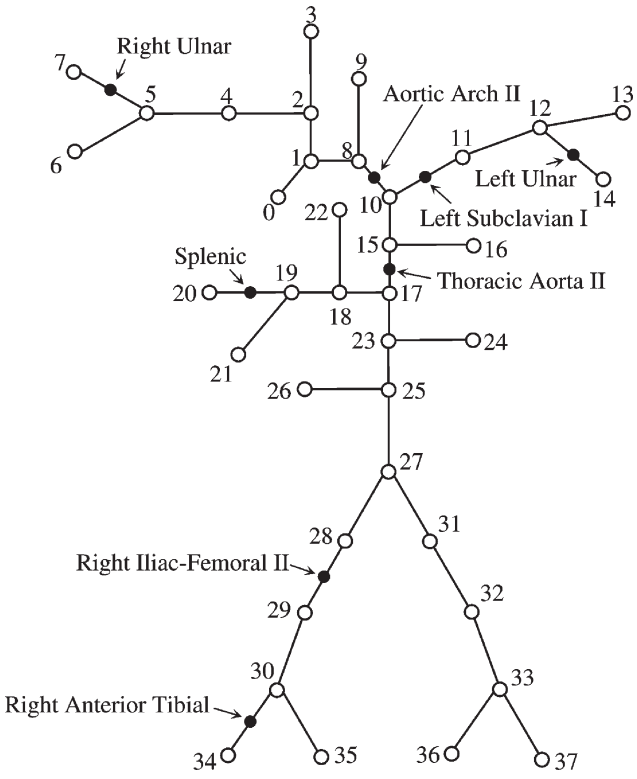

Fig. 3. Scheme of 37-segment arterial tree. The node number zero denotes the arterial tree inlet, where a periodic flow rate was prescribed. Filled circles denote measurement sites

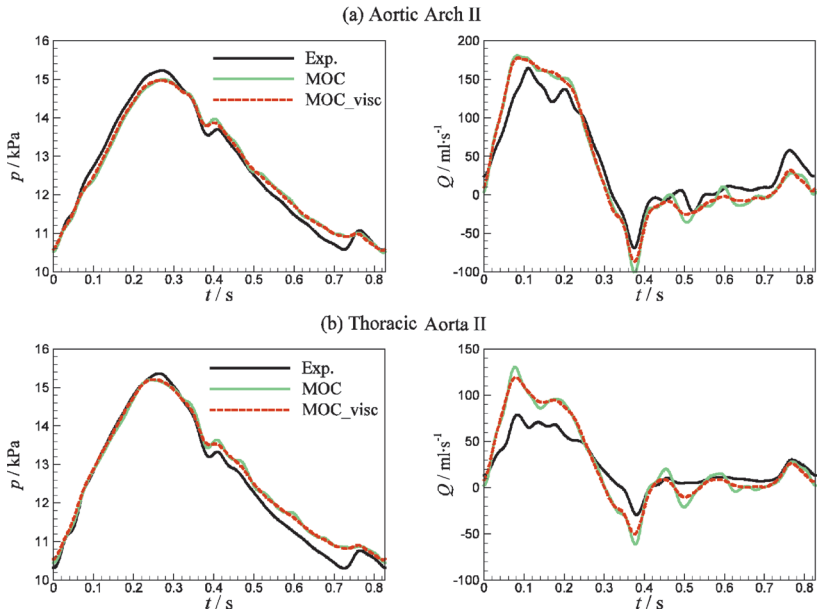

Fig. 4. 37-artery network. Pressure (left) and flow rate (right) at midpoints of two arterial segments: (a) Aortic Arch II and (b) Thoracic Aorta II. Black solid lines represent in vitro experimental data (Exp.), green solid lines denote numerical results of the developed method with elastic arterial wall (MOC), and red dashed lines denote numerical results of the method of characteristics with viscoelastic arterial wall (MOC_visc) [4]

Table 1. Percentage RMS errors of the calculated pressure and flow rate with respect to the measurements at the locations indicated in Fig. 3, and the range of these errors from six other numerical schemes

Arterial segment	Numerical scheme		ε_p^{RMS}	ε_Q^{RMS}
Aortic arch II	Six schemes	min	1.68	12.02
		max	1.94	12.34
	MOC		1.77	12.47
	MOC – visc.		1.56	11.89
Thoracic aorta II	Six schemes	min	2.17	25.26
		max	2.53	25.62
	MOC		2.26	26.27
	MOC – visc.		2.15	24.50
Left subcl. I	Six schemes	min	3.05	13.87
		max	3.12	14.45
	MOC		3.19	14.39
	MOC – visc.		3.04	13.53
R. iliac-femoral II	Six schemes	min	3.65	23.90
		max	3.97	24.80
	MOC		3.97	26.02
	MOC – visc.		3.68	22.52
Left ulnar	Six schemes	min	2.57	12.42
		max	2.75	12.91
	MOC		2.67	12.81
	MOC – visc.		2.28	11.36
R. anter. tibial	Six schemes	min	3.21	9.88
		max	3.43	11.05
	MOC		3.90	10.98
	MOC – visc.		3.15	8.15
Right ulnar	Six schemes	min	2.42	11.22
		max	2.66	11.73
	MOC		2.62	11.84
	MOC – visc.		2.53	10.70
Splenic	Six schemes	min	2.22	9.02
		max	2.36	9.79
	MOC		2.52	10.37
	MOC – visc.		1.93	7.80

method is implicit, unconditionally stable and capable of dealing with nonlinearities.

At the inlet node the pressure or the inflow can be prescribed. In all simulations, the initial conditions were $Q(x,0)=0$, $A(x,0)=A_0$ and $p(x,0)=p_0$. The integration time should be long enough to achieve cycle-to-cycle periodicity, and the last cycle is examined.

Results and discussion

Fig. 3 schematically shows the examined network. All data relevant to this problem are provided in the supplement material [6]. In the performed simulation each segment was divided into a number of elements (total number of elements was 431), and integration time step was 1 ms. Fig. 4 shows the comparison of the measured and calculated pressure and flow (for the case of elastic and viscoelastic wall), and Table 1 shows the percentage root mean square (RMS) errors of the calculated results with respect to the experimental data of the developed method and the range of these errors from the six other methods examined in [6].

In the case of elastic wall, most of the MOC errors are very similar in size to errors from six numerical schemes (see Table 1). In the case of viscoelastic wall, the pressure and flow RMS errors are slightly reduced, and a reduction in peak values of pressure and flow rate is achieved (that is closer to experimental data) because of damping high frequency oscillations.

References

[1] Ottesen, JT, Olufsen, MS, Larsen, JK. *Applied mathematical models in human physiology*. SIAM: Society for Industrial and Applied Mathematics, 2004.

[2] van de Vosse FN, Stergiopulos N. Pulse wave propagation in the arterial tree. *Annual Review of Fluid Mechanics* 2011; **43**(1): 467–499. DOI: 10.1146/annurev-fluid-122109-160730.

[3] Korade I, Virag Z, Šavar M. Numerical simulation of one-dimensional flow in elastic and viscoelastic branching tube. *Proceedings of the 6th European Conference of Computational Fluid Dynamics (ECFD VI)*, Oñate E, Oliver X, Huerta A (ur). International Center for Numerical Methods in Engineering (CIMNE): Barcelona, Spain, July 20-25, 2014; 7124–7131.

[4] Korade I, Modeliranje strujanja krvi u arterijskom stablu s viskoelastičnom stijenkom (eng. Modeling of Blood Flow in an Arterial Tree with Viscoelastic Wall), PhD, University of Zagreb, Faculty of Mechanical Engineering and Naval Architecture, 2017.

[5] Matthys KS, Alastruey J, Peiró J, Khir AW, Segers P, Verdonck PR, Parker KH, Sherwin SJ. Pulse wave propagation in a model human arterial network: Assessment of 1-D numerical simulations against in vitro measurements. *Journal of Biomechanics* 2007; 40 (15):3476–3486. doi:10.1016/j.jbiomech.2007.05.027.

[6] Boileau E, Nithiarasu P, Blanco PJ, Müller LO, Fossan FE, Hellevik LR, Donders WP, Huberts W, Willemet M, Alastruey J. A benchmark study of numerical schemes for one-dimensional arterial blood flow modelling. *International Journal for Numerical Methods in Biomedical Engineering* 2015; 31(10):e02732 (33 pages). doi:10.1002/cnm2732.